Hindawi
Journal of Nanomaterials
Volume 2017, Article ID 2738015, 8 pages
https://doi.org/10.1155/2017/2738015

Research Article

Optical Design of Porous ZnO/TiO_2 Films for Highly Transparent Glasses with Broadband Ultraviolet Protection

Han Sung Song,[1] Young Jin Yoo,[1] Gil Ju Lee,[1] Ki Soo Chang,[2] and Young Min Song[1]

[1]*School of Electrical Engineering and Computer Science, Gwangju Institute of Science and Technology, 123 Cheomdan-gwagiro, Buk-gu, Gwangju 61005, Republic of Korea*
[2]*Center for Analytical Instrumentation Development, Korea Basic Science Institute, 169-148 Gwahak-ro, Yuseong-gu, Daejeon 306-806, Republic of Korea*

Correspondence should be addressed to Young Min Song; ymsong@gist.ac.kr

Received 16 June 2017; Revised 27 September 2017; Accepted 15 October 2017; Published 8 November 2017

Academic Editor: Tao Gong

We present a design of a bilayer porous film structure on a glass substrate for the highly efficient ultraviolet (UV) protection with high visible-light transparency. To effectively block UVB (280–315 nm) and UVA (315–400 nm), titanium dioxide (TiO_2) and zinc oxide (ZnO) are used as absorbing layers having the appropriate coverages in different UV ranges with extinction coefficients, respectively. We show the process of refractive index (RI) matching by controlling porosity (P_r). Effective RIs of porous media with TiO_2 and ZnO were calculated based on volume averaging theory. Transmittances of the designed films with different effective RIs were calculated using rigorous coupled-wave analysis method. Using admittance loci method, the film thickness was optimized in center wavelengths from 450 to 550 nm. The results show that the optimal design provides high UV shielding performance at both UVA and UVB with high transparency in the visible range. We also analyze electrical field distributions in each layer and angle dependency with 3D HSV color map.

1. Introduction

Various harmful effects of ultraviolet (UV) rays from sunlight have been reported in many years. In general, UVA (315–400 nm in wavelength) induces optical degradation and yellowing of polymers, cracking, blistering of wood, and skin aging by generating reactive oxygen species [1–3]. An overexposure to UVB (280–315 nm) causes the skin cancer as the radiation directly damages DNA in skin cells, and it also leads optical degradation and yellowing damage of polymers, pigments, dyes, and semiconductor devices [1, 4–7]. Relatively, the harmful effects of UVB are more fatal than UVA due to its higher photon energy. Thus, to prevent such damage, protecting against both of UV has garnered interest in the research and development of new materials and optical structures.

For UV protection, inorganic UV absorbers (TiO_2, ZnO, CeO_2, etc.) are generally used, which have been studied in various UV shielding applications [8–11]. These materials efficiently absorb the UV radiation by excitation of electrons since their wide bandgap corresponds to the wavelength of UV. Representatively, ZnO has the UV absorptivity in both UVB and UVA due to the relatively low band gap energy of 3.31 eV, whereas TiO_2 has strong absorption only at UVB due to the relatively high band gap energy of 3.5 eV. Although organic UV absorbers were also used for UV protection to materials or skin, there is a limitation for application to embed the absorbers due to the low stability of the extensively used polymer matrices upon irradiation with UV light [12, 13]. Typically, UV shielding is often required together with high visible-light transparency in applications such as safety glasses, automobiles, and windows [9]. In visible light, UV absorbing materials transmit light but produce reflection loss caused by their high refractive indices (RIs). For UV protecting with high visible-light transparency, it is required to alleviate the effects of the high RI of the UV absorbers.

In recent years, as the synthesis of nanoparticles and nanofabrication have been developed, several studies to achieve high transmittance by using nanostructures have been reported that are nanoporous film [14], nanorod arrays [15],

nanoparticles [16], and tapered nanostructures [17]. Using these nanomaterials, the medium can obtain the porosity (P_r) to reduce high RI causing optical loss with Fresnel reflection. In UV protective applications, transparent coatings in visible lights with UV blocking can also be realized by using these nanomaterials [18]. To achieve high transparency in visible light, high RIs of UV absorbers can be lowered by applying P_r with various nanostructures. Unfortunately, as P_r increases in UV absorptive materials, the extinction coefficients in UV region also decrease, causing reduced UV absorption. To compensate this degradation, different UV absorbers with high extinction coefficients in each UV region (i.e., UVA and UVB) are used in the form of nanocomposites or multilayer structures [19, 20]. However, despite several studies of nanostructures for transparent UV protection, optical analysis and design have hardly been conducted to optimize UV absorbers for high visible-light transparency, and only studies adopting the reflection effect such as 1D photonic crystal or Bragg mirror have been conducted [21–23].

In this study, we propose a design that adopts bilayer of the absorbers TiO_2 and ZnO as an antireflection coating with different RIs to improve the transparency in the visible range with UV protection. We use the volume averaging theory [24] to calculate the RIs of the porous structure and the admittance loci method to optimize the coating thickness [25]. Based on the rigorous coupled-wave analysis (RCWA) method, we calculate the transmittance of the designed bilayer films and discuss the optimum structure as a compromise between UV protection and visible-light transparency.

2. Results and Discussion

Figure 1(a) shows the schematic of our design for transparent coating layers with UV blocking. The designed coating layer consists of TiO_2 and ZnO porous layers as UV shielding layers on a glass substrate. We adopted BK7 glass as a commonly used transparent glass substrate without UV blocking. The UV blocking performance of each layer is determined from absorbing properties of TiO_2 and ZnO, which have band gaps and the absorption edges reported to be 3.5 eV and 3.31 eV, respectively. Therefore, in our proposed films, TiO_2 layer absorbs UVB corresponding to the photon energy of 3.94–4.43 eV and the UVA region (3.10–3.94 eV) is blocked by the absorption of ZnO layer. To observe the absorption in different wavelengths, the extinction coefficients of TiO_2 and ZnO are presented with UV regions, as depicted in Figure 1(b) [26, 27]. Although ZnO has extinction coefficients in both UVA and UVB, the porous ZnO is insufficient to completely block UVB, which is more harmful than UVA, due to its reduced extinction coefficient. As a solution, TiO_2 is used as an additional UVB absorber, which has high extinction coefficients in UVB. However, since the UV absorbers have much higher refractive indices (RIs) compared with bare glass in visible wavelengths, as shown in the inset of Figure 1(b), the difference in RI of each material Δn is 0.8 and 0.5 at 550 nm wavelength, which results in strong Fresnel reflection. To reduce the effective RI, we applied porosity (P_r) to UV absorbers. Figure 1(c) shows the index profiles (at 550 nm) of the nonporous and our porous film. To improve transmittance with UV shielding effect, applying P_r 70% to TiO_2 (TiO_2 P_r 70%) and P_r 80% to ZnO (ZnO P_r 80%), the RI of the TiO_2 (n_2) layer decreased from 2.3 to 1.51 and that of the ZnO layer (n_1) also decreased to 1.27 at 550 nm wavelength. Our design has been optimized in antireflective conditions with P_rs and thicknesses, and the detailed process will be discussed below (see Figures 2 and 3). Figure 1(d) shows the transmission characteristics of our design, calculated by RCWA method, with the transmittance of each UV absorbing monolayers. As a result, the bilayer coating performed high transmittance (about 90%) with effective UV blocking more than 90%. The bilayer coating consisting of TiO_2 P_r 70% and ZnO P_r 80% (red) has similar transmittance to ZnO P_r 80% single layer (light violet) at UVA and visible region and it blocks wider range of UV effectively than both single layer films of TiO_2 P_r 70% (light green) and ZnO P_r 80% film. For comparison, the transmittance of nonporous films was also plotted in the Figure 1(d) inset. The transmittance of our film is higher than nonporous TiO_2 (dark green) and ZnO (dark violet) in the visible region, with comparable UV blocking.

Basically, to improve transmittance of the film structure with the antireflective condition, the RI and the thickness of the antireflection layer should be considered. Since the optimal thickness for the antireflective condition depends on the RI as shown in $d = \lambda/4n_c$, the RI corresponding to the antireflective condition should be preferentially optimized. To observe the variation of the effective index with P_r, we calculated RIs and extinction coefficients of both TiO_2 and ZnO with P_r based on volume averaging theory [24], as depicted in Figure 2. The results show that as P_r increases, not only do the high RIs of TiO_2 and ZnO tend to decrease but extinction coefficients of them for UV absorption also tend to decrease. Ideally, multiple layers can be formed as antireflective layers in a multilayered coating; however, RIs of antireflective layers considerably lower than the substrate are required. In our structure, high P_r's to achieve low RIs with multilayered antireflective layers result in largely reduced extinction coefficients causing difficulty in UV shielding. Therefore, applying P_rs, we matched the RI of TiO_2 layer, relatively high RI, to the substrate and exploited a ZnO layer with a relatively low RI as a single antireflective layer. To satisfy the antireflective condition of single layer relating to the RI as $n_1 = \sqrt{n_2 n_{\text{air}}}$, the RI of the antireflective coating layer, n_1, should be lower than the RI of the substrate, n_2. In Figure 2(a), the dashed line represents the points where $n = 1.5$ similar to the RI of glass substrate. To match with the RI of the glass substrate, lower P_r is required in ZnO than in TiO_2. Therefore, as an antireflective layer, ZnO is advantageous for achieving lower RI of glass compared to TiO_2. From these results, we selected optimum P_rs of TiO_2 and ZnO as 70% and 80%, respectively, with RI of 1.518 and 1.271 at 550 nm wavelength, almost satisfying the antireflective condition. Figure 2(b) shows extinction coefficient for each UV region separated with dash-dot line. The wavelength corresponding to the maximum extinction coefficient for each UV region remains unchanged. Therefore, the extinction coefficients of TiO_2 P_r 70% and ZnO P_r 80% are 0.3 at UVB (310 nm) and 0.2 at UVA (360 nm), respectively, and they are enough to block each UV region by optimizing thicknesses.

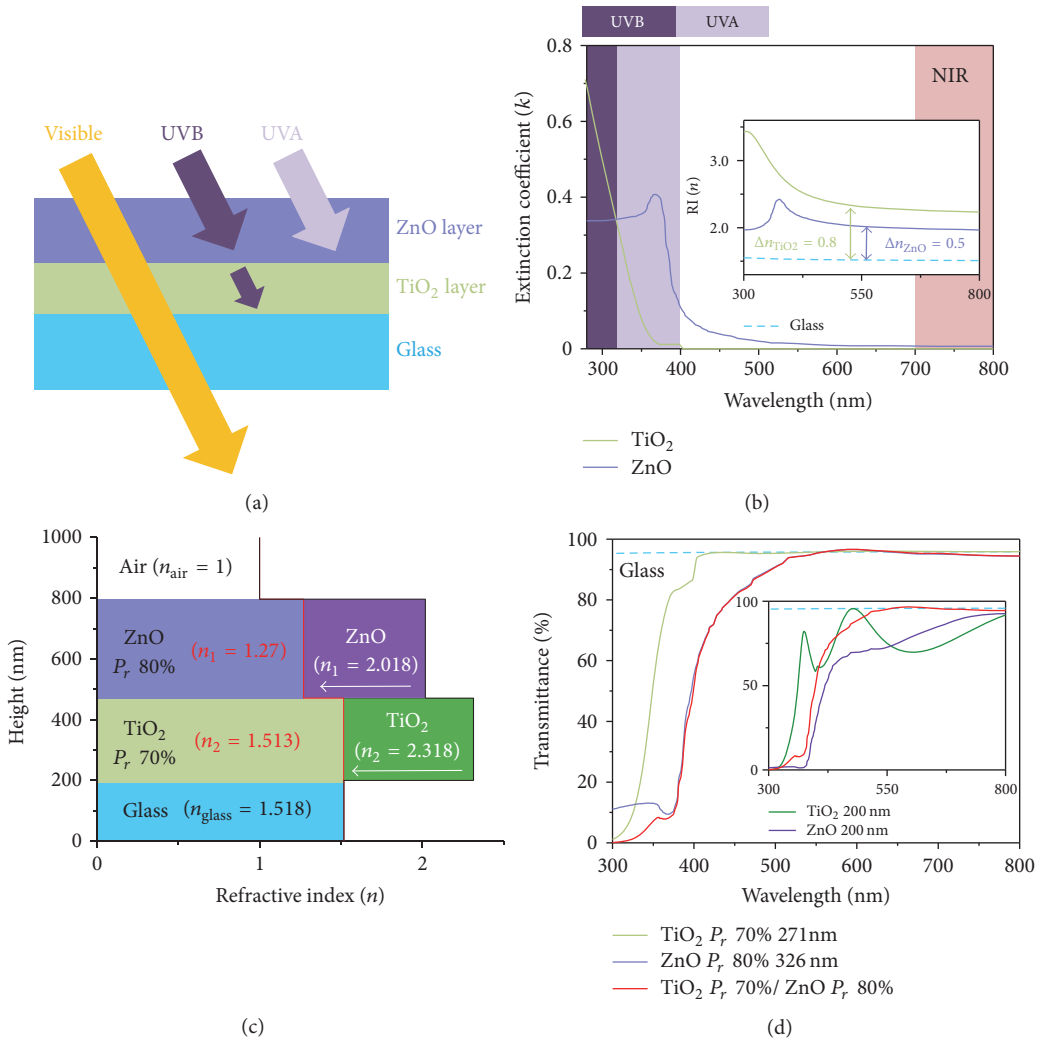

FIGURE 1: (a) Schematic illustration of the designed film for transparent UV protection. (b) Extinction coefficients of TiO_2 and ZnO. The inset shows refractive indices (RIs) of TiO_2 and ZnO [26, 27]. (c) RI profiles versus height of UV absorbing film (left) and UV absorbing film with porosity (P_r). (d) The calculated transmittance of the layer coating of TiO_2 P_r 70% and ZnO P_r 80% and bilayer film with them stacked as a function of wavelength. The inset of (d) shows the transmittance of the nonporous single layer film and designed film.

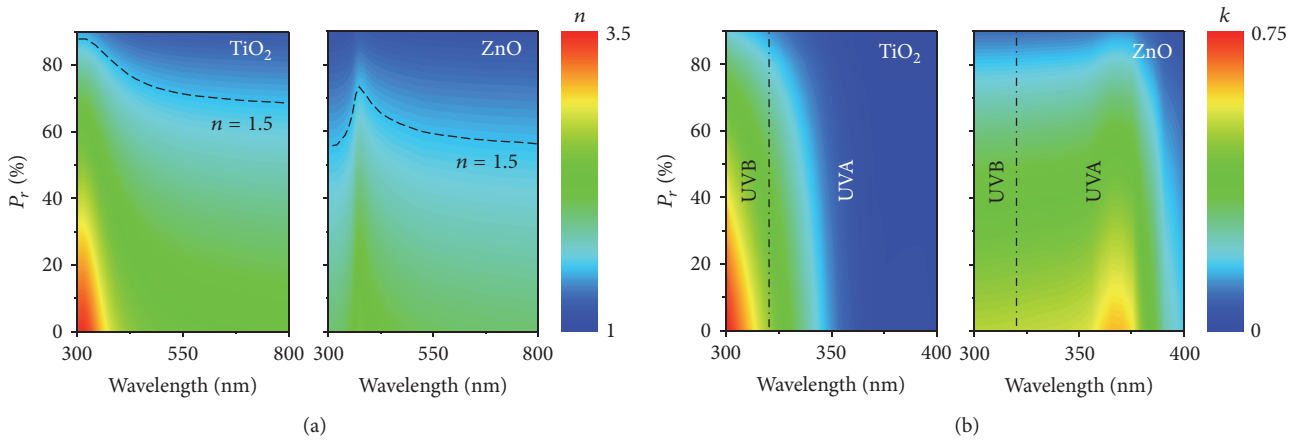

FIGURE 2: Contour plot of the (a) RI (n) and (b) extinction coefficient (k) of TiO_2 and ZnO as a function of P_r and wavelength.

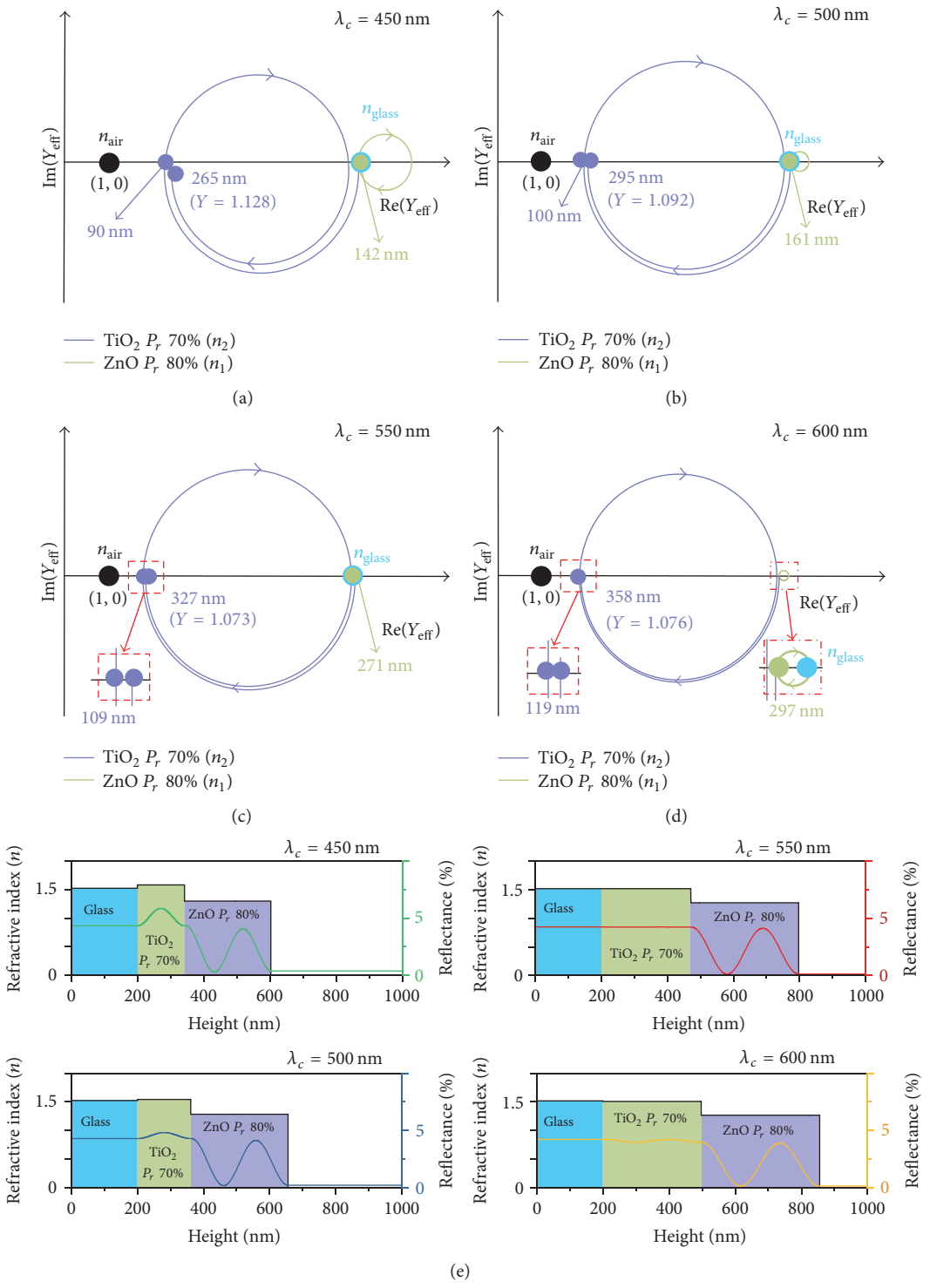

FIGURE 3: Admittance diagrams of UV absorbing films designed with different center wavelengths (λ_c) of (a) 450, (b) 500, (c) 550, and (d) 600 nm. (e) Schematic illustrations of RI profiles and reflectance versus thicknesses of the films.

To optimize the thicknesses of the coating layers composed of TiO_2 P_r 70% and ZnO P_r 80%, we used the admittance loci method based on an optical simulation using Macleod (Thin Film Center, Inc.) [25]. In thin-film optics, the reflectance can be expressed as $R = [(1 - Y)/(1 + Y)]^2$, where Y is the optical admittance defined as the ratio of the magnetic and electric fields tangential to the surface. Since the optimum thickness to satisfy the antireflection condition depends on the wavelength, we calculated the admittance diagram at different center wavelengths of 450, 500, 550, and 600 nm (Figures 3(a)–3(d)). In admittance diagram, starting from the end point of admittance at each layer, the locus of

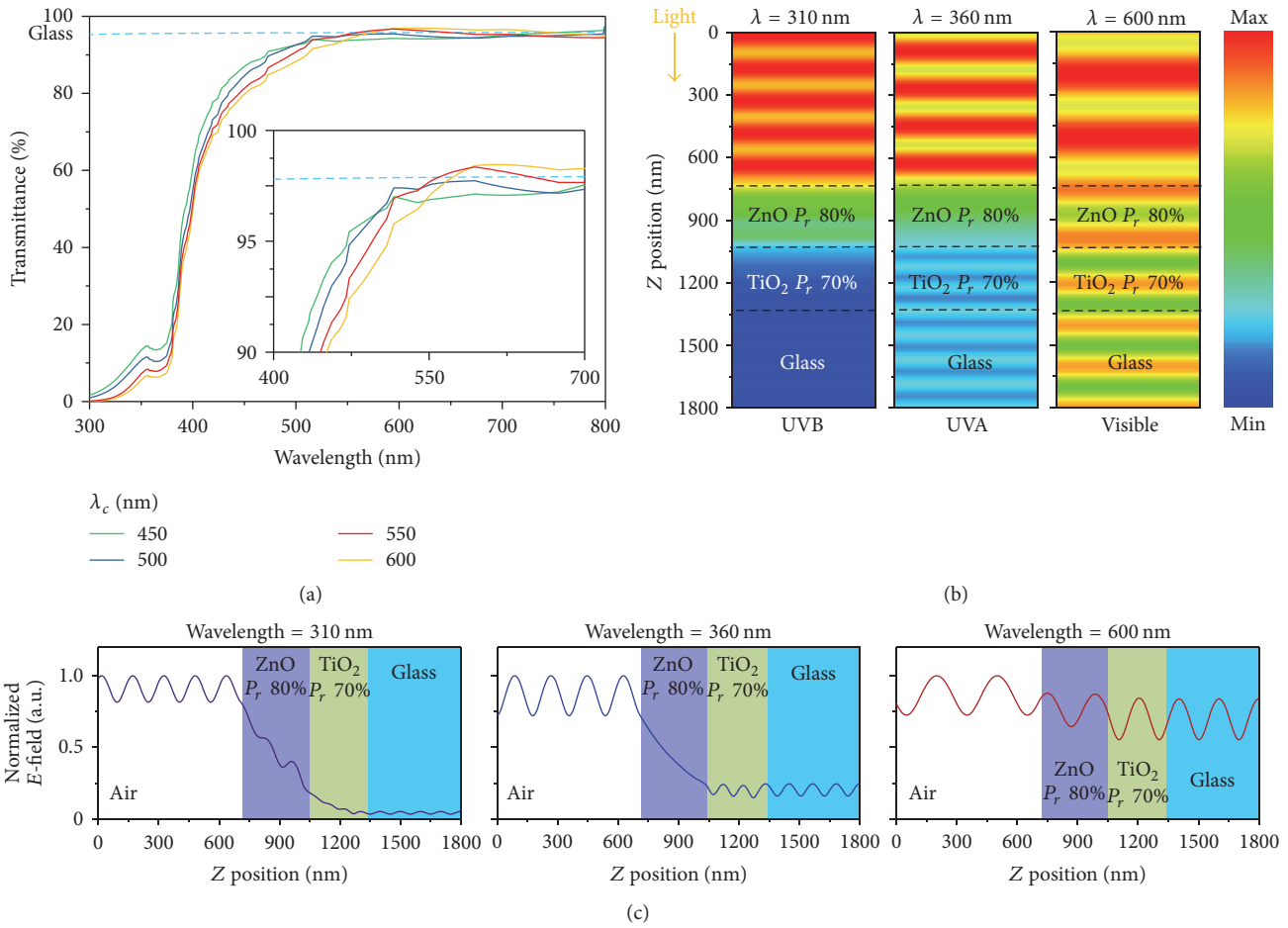

FIGURE 4: (a) Transmittance spectra of UV absorbing film as a function of wavelength with different center wavelengths (i.e., λ_c = 450, 500, 550, and 600 nm). The inset highlights the visible region. (b) Electric field intensity distribution of the designed film with a center wavelength of 550 nm at UVB (λ = 310 nm), UVA (λ = 360 nm), and visible (λ = 600 nm), respectively. (c) The normalized electric field intensities versus the Z position of (b) are presented as a line graph.

upper layer repeatedly rotates in a clockwise direction with increasing film thickness. Fundamentally, zero reflectance can only be obtained where the locus of admittance reaches the point of air (1, 0), and, in general cases, the reflectance is minimized near the points $(Y, 0)$ closer to that of air. At λ_c = 450 nm, the optimum thickness of the TiO$_2$ P_r 70% and ZnO P_r 80% is 142 nm and 265 nm, respectively (Figure 3(a)). The admittance is 1.128, the highest among the films due to the RI of TiO$_2$ P_r 70%, n_2, higher than that of glass ($n_{\text{glass}} < n_2$, $\Delta n \fallingdotseq 0.08$). For the same reason, at λ_c = 500 nm, the admittance was calculated as 1.092 but it was lower than that of the film with λ_c = 450 nm because of the lower difference of RI $\Delta n \fallingdotseq 0.023$. The film with λ_c = 500 nm is composed of 161 nm thickness of TiO$_2$ P_r 70% and 295 nm thickness of ZnO P_r 80% (Figure 3(b)). For the other cases, $n_{\text{glass}} > n_2$, admittance reached closer to the admittance point of the air than previous cases. The coating optimized at λ_c = 550 nm is ZnO P_r 80% 327 nm/TiO$_2$ P_r 70% 271 nm (Figure 3(c)). Although n_2 decreases at longer λ_c, the admittance was minimized as 1.073, since the RIs of ZnO P_r 80% (n_1) and TiO$_2$ P_r 70% (n_2) satisfy the condition $n_1 = \sqrt{n_2 n_{\text{air}}}$ at λ_c = 550 nm. The film optimized at λ_c = 600 nm has the admittance 1.076 higher than that of film with λ_c = 550 nm (Figure 3(d)). Figure 3(e) represents reflectance spectra converted from admittance and thickness of the coatings at each λ_c. For sufficient absorption of the TiO$_2$ P_r 70% and ZnO P_r 80% layers with different λ_c, we chose the film thickness with the second dip in the reflectance spectra of bilayer coating. Each of the optimal thicknesses shows nearly zero reflection at all wavelengths of each center. Specifically, since the RI of TiO$_2$ became lower than that of glass at λ_c > 550 nm, the increment in the thickness of the TiO$_2$ layer was larger with variations in center wavelength from 450 to 550 nm.

To compare the performances of the films with different center wavelengths, we plotted the transmittance of the films in Figure 4(a) and we also present the transmittance values at the UVB, UVA, and visible regions in Table 1. From the relation between λ_c and the thickness of each layer where the reflectance is minimized, the absorbing effects of the designed film also increased with increasing λ_c. Therefore, the transmittance at UVB gradually decreases from 2.78% to 0.2% as λ_c increased. Similarly, the UVA transmittance gradually

Table 1: Transmittances of UV absorbing films with different center wavelengths (i.e., 450, 500, 550, and 600 nm) at different regions (i.e., UVB, UVA, and visible).

Center wavelength (nm)	450	500	550	600
T (%)				
UVB (310 nm)	2.78	1.76	0.35	0.20
UVA (360 nm)	13.80	10.84	8.05	6.48
Visible (avg 400–700 nm)	90.84	90.43	89.95	89.23

decreases from 13.80 to 6.48% and the difference between the maximum and minimum transmittance depending on λ_c was over 7%. The average transmittance in the visible range decreases from 90.84% to 89.23%. To observe the UV absorbing effect of the designed film, we calculated the electrical field distributions of the optimized films at λ_c = 550 nm showing adequate UV blocking in both UVA and UVB (Figure 4(b)). The full lines in Figure 4(b) represent interfaces of the layers and the amplitude of the electric field at the UVB region (λ = 310 nm) dropped in both the ZnO P_r 80% and TiO_2 P_r 70% layers propagating to the glass. For the λ = 360 nm case, a decrease of amplitude appeared only in the ZnO P_r 80% layer. At the visible region (λ = 600 nm), although there was a slight decline in amplitude by the absorption of ZnO P_r 80%, the amplitude was maintained while passing through the film. To observe in more detail, the normalized amplitude spectra of electric field were plotted as a function of Z position, as shown in Figure 4(c). At the dark blue shaded region (ZnO P_r 80% layer), the amplitude of UVB and UVA decayed exponentially. Similarly, the electric field of UVB decreased at the green shaded region (TiO_2 P_r 70% layer). However, since TiO_2 P_r 70% has a low extinction coefficient in that region, a gradual decrease in UVA is observed. In case of the visible light, the amplitude was only slightly off in the dark blue shaded area (ZnO P_r 80% layer).

Furthermore, we considered the angular dependency of the designed films. The transmittance values of the films and bare glass were calculated for an incident angle from 0 to 80° in the wavelength range of 300–800 nm. In the contour diagram of Figure 5(a), the designed films exhibit an angle dependence of transmittance comparable to that of bare glass in visible light, while UV absorption is maintained regardless of incident angles. Especially in the longer wavelengths, the high transmittance region of each designed film is extended compared to that of the bare glass. Additionally, to evaluate the visible-light transparency in terms of color, we represented RGB colors for different incident angles of the proposed films and bare glass. Both the designed films and the bare glass show more blurred colors at higher incident angles. For quantitative comparison in terms of color, we plotted HSV (hue, saturation, and value) color map. For normal incidence, the color of films is almost the same at the adjacent point of pure white point (0, 0, 100), which means colorless transmitted light. However, at higher incident angles, the film calculated at λ_c = 550 nm showed the closest color to white and also was most similar to glass colors.

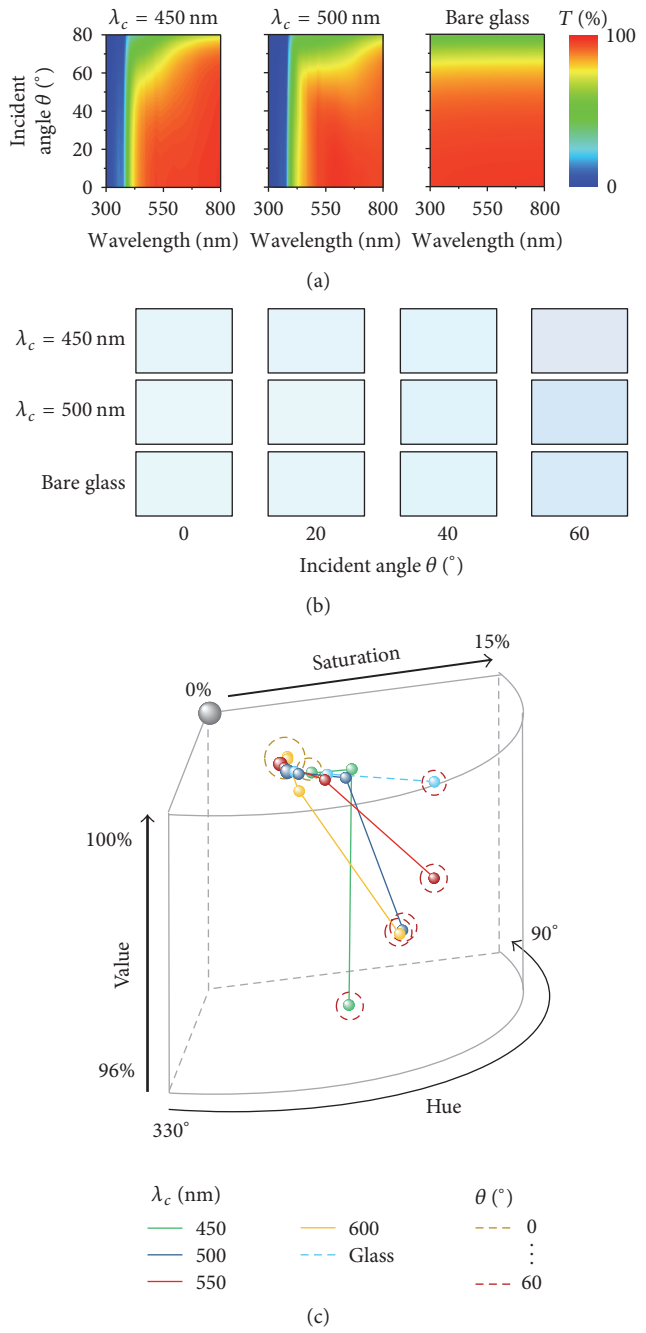

Figure 5: (a) Contour plots of angle-resolved transmittance (T) comparing films with different center wavelengths (λ_c = 450 and 550 nm) and glass as a function of wavelength. (b) Color representations from the calculated transmittance of the films with λ_c = 450 and 550 nm and bare glass. (c) 3D HSV (i.e., hue, saturation, and value) color map of the films with different center wavelengths (λ_c = 450, 500, 550, and 600 nm) at an incident angle from 0 to 60° with an increment of 20°.

3. Conclusions

In this work, we designed the transparent UV shielding films composed of TiO_2 and ZnO by calculation using the RCWA method. The bilayered structure was achieved in the high

transmittance by applying P_r to lower the high RI of the UV absorbing layer and optimize the thickness. Our structure almost completely blocks UVB ($T_{310\,nm} \sim 0.35\%$) and also blocks UVA with very low transmittance ($T_{360\,nm} \sim 8\%$), while maintaining the transmittance at about 90% in the visible region. We believe that the design guidelines of UV shielding films can be used for various applications including the coatings to protect flexible devices, epidermal devices, paints, wood, and polymers from harmful effects due to both UVA and UVB.

Conflicts of Interest

The authors declare that there are no conflicts of interest regarding the publication of this paper.

Authors' Contributions

H. S. Song and Y. J. Yoo equally contributed to this work.

Acknowledgments

This research was supported by the Korea Basic Science Institute under the R&D program (D37615) supervised by the Ministry of Science, ICT and Future Planning and by Creative Materials Discovery Program through the National Research Foundation of Korea (NRF) funded by Ministry of Science and ICT (NRF-2017M3D1A1039288).

References

[1] A. L. Andrady, S. H. Hamid, X. Hu, and A. Torikai, "Effects of increased solar ultraviolet radiation on materials," *Journal of Photochemistry and Photobiology B: Biology*, vol. 46, no. 1-3, pp. 96–103, 1998.

[2] P. Hayoz, W. Peter, and D. Rogez, "A new innovative stabilization method for the protection of natural wood," *Progress in Organic Coatings*, vol. 48, no. 2-4, pp. 297–309, 2003.

[3] H. Yasui and H. Sakurai, "Age-dependent generation of reactive oxygen species in the skin of live hairless rats exposed to UVA light," *Experimental Dermatology*, vol. 12, no. 5, pp. 655–661, 2003.

[4] L.-E. Wang, C. Li, S. S. Strom et al., "Repair capacity for UV light-induced DNA damage associated with risk of non-melanoma skin cancer and tumor progression," *Clinical Cancer Research*, vol. 13, no. 21, pp. 6532–6539, 2007.

[5] M. Moehrle, "Outdoor sports and skin cancer," *Clinics in Dermatology*, vol. 26, no. 1, pp. 12–15, 2008.

[6] D. Alshiyab, C. Edwards, M. F. Chin, and A. V. Anstey, "Targeted ultraviolet B phototherapy: Definition, clinical indications and limitations," *Clinical and Experimental Dermatology*, vol. 40, no. 1, pp. 1–5, 2015.

[7] M. Jørgensen, K. Norrman, and F. C. Krebs, "Stability/degradation of polymer solar cells," *Solar Energy Materials & Solar Cells*, vol. 92, no. 7, pp. 686–714, 2008.

[8] M. Aklalouch, A. Calleja, X. Granados et al., "Hybrid sol-gel layers containing CeO2 nanoparticles as UV-protection of plastic lenses for concentrated photovoltaics," *Solar Energy Materials & Solar Cells*, vol. 120, pp. 175–182, 2014.

[9] E. Lizundia, L. Ruiz-Rubio, J. L. Vilas, and L. M. León, "Poly(l -lactide)/zno nanocomposites as efficient UV-shielding coatings for packaging applications," *Journal of Applied Polymer Science*, vol. 133, no. 2, Article ID 42426, 2016.

[10] M. S. Ghamsari, S. Alamdari, W. Han, and H.-H. Park, "Impact of nanostructured thin ZnO film in ultraviolet protection," *International Journal of Nanomedicine*, vol. 12, pp. 207–216, 2017.

[11] A. P. Popov, A. V. Priezzhev, J. Lademann, and R. Myllylä, "TiO2 nanoparticles as an effective UV-B radiation skin-protective compound in sunscreens," *Journal of Physics D: Applied Physics*, vol. 38, no. 15, pp. 2564–2570, 2005.

[12] J. Keck, M. Roessler, C. Schroeder et al., "Ultraviolet absorbers of the 2-(2-hydroxyaryl)-l,3,5-triazine class and their methoxy derivatives: Fluorescence spectroscopy and X-ray structure analysis," *The Journal of Physical Chemistry B*, vol. 102, no. 36, pp. 6975–6985, 1998.

[13] F. Gugumus, "Possibilities and limits of synergism with light stabilizers in polyolefins 2. UV absorbers in polyolefins," *Polymer Degradation and Stability*, vol. 75, no. 2, pp. 309–320, 2002.

[14] B. Wang, J. S. Price, and N. C. Giebink, "Durable broadband ultralow index fluoropolymer antireflection coatings for plastic optics," *Optica*, vol. 4, no. 2, pp. 239–242, 2017.

[15] Y. Gao, I. Gereige, A. El Labban, D. Cha, T. T. Isimjan, and P. M. Beaujuge, "Highly transparent and UV-resistant superhydrophobic SiO2-coated ZnO nanorod arrays," *ACS Applied Materials & Interfaces*, vol. 6, no. 4, pp. 2219–2223, 2014.

[16] J. Y. Y. Loh, D. P. Puzzo, P. G. O'Brien, G. A. Ozin, and N. P. Kherani, "Enhancing photovoltaics with broadband high-transparency glass using porosity-tuned multilayer silica nanoparticle anti-reflective coatings," *RSC Advances*, vol. 4, no. 59, pp. 31188–31195, 2014.

[17] K. Choi, Y. Yoon, J. Jung et al., "Antireflective films: super-antireflective structure films with precisely controlled refractive index profile," *Advanced Optical Materials*, vol. 5, no. 3, 2017.

[18] Y. Tu, L. Zhou, Y. Z. Jin et al., "Transparent and flexible thin films of ZnO-polystyrene nanocomposite for UV-shielding applications," *Journal of Materials Chemistry*, vol. 20, no. 8, pp. 1594–1599, 2010.

[19] I. Lee, S. Gim, J. Y. Park, S. J. Kim, and J.-L. Lee, "One-Structure-Based Barrier Film for Simultaneous Exclusion of Water and Ultraviolet Light," *Advanced Optical Materials*, vol. 5, no. 3, Article ID 1600888, 2017.

[20] J. R. C. Smirnov, M. E. Calvo, and H. Míguez, "Selective UV reflecting mirrors based on nanoparticle multilayers," *Advanced Functional Materials*, vol. 23, no. 22, pp. 2805–2811, 2013.

[21] J. R. C. Smirnov, M. Ito, M. E. Calvo et al., "Adaptable Ultraviolet Reflecting Polymeric Multilayer Coatings of High Refractive Index Contrast," *Advanced Optical Materials*, vol. 3, no. 11, pp. 1633–1639, 2015.

[22] H. Cui, M. Zayat, P. G. Parejo, and D. Levy, "Highly efficient inorganic transparent UV-protective thin-film coating by low temperature sol-gel procedure for application on heat-sensitive substrates," *Advanced Materials*, vol. 20, no. 1, pp. 65–68, 2008.

[23] W. S. Choi, E. J. Kim, S. G. Seong, Y. S. Kim, C. Park, and S. H. Hahn, "Optical and structural properties of ZnO/TiO2/ZnO multi-layers prepared via electron beam evaporation," *Vacuum*, vol. 83, no. 5, pp. 878–882, 2009.

[24] A. Garahan, L. Pilon, J. Yin, and I. Saxena, "Effective optical properties of absorbing nanoporous and nanocomposite thin films," *Journal of Applied Physics*, vol. 101, no. 1, Article ID 014320, 2007.

[25] H. A. Macleod, *Thin-Film Optical Filters*, Institute of Physics Publishing, London, UK, 4th edition, 1986.

[26] S. Y. Kim, "Simultaneous determination of refractive index, extinction coefficient, and void distribution of titanium dioxide thin film by optical methods," *Applied Optics*, vol. 35, no. 34, pp. 6703–6707, 1996.

[27] H. Yoshikawa and S. Adachi, "Optical Constants of ZnO," *Japanese Journal of Applied Physics*, vol. 36, no. Part 1, No. 10, pp. 6237–6243, 1997.